Original paper

Monte Carlo dosimetry for a new ^{32}P brachytherapy source using FLUKA code

Razieh Rajabi, MSc, Payvand Taherparvar, PhD

Department of Physics, Faculty of Science, University of Guilan, Rasht, Iran

Abstract

Purpose: Dosimetric characterization of a new 32P brachytherapy source was studied and the validity of the FLUKA code to reproduce the dosimetric parameters in a water phantom was evaluated. In addition, dose rate distributions around the 32P source sheathed by a catheter and unsheathed source were investigated in different tissue phantoms.

Material and methods: The new 32P source was modeled using FLUKA Monte Carlo code. According to the AAPM TG-60 recommendations, reference of absorbed dose rate, radial dose function, anisotropy function, and an away-along table for quality assurance purposes inside water phantom were calculated. Moreover, the results of the radial dose function and dose rate were obtained for the sheathed source and unsheathed sources at radial distances in different tissue phantoms: liver, fat tissue, 9-component soft tissue, and 4-component soft tissue.

Results: The calculated dosimetric parameters of the new 32P source by FLUKA code in water phantom agreed well with that of the GEANT4 calculation. The 2D away-along dose results were similar to the GEANT4 simulation for distances less than 0.25 cm, small differences were apparent at long distances from the source. Dose rate evaluation for the sheathed source shows that the presence of a catheter increases the dose values up to 2.11% in comparison with the unsheathed source in water phantom. Our results show that the radial dose function calculated in water, as generalized by AAPM TG-60, differed in tissue, especially at large distances from the source.

Conclusions: This work fully characterizes dosimetric parameters of the sheathed and unsheathed new 32P brachytherapy sources in water and different tissue phantoms by using FLUKA code. The results demonstrate that the dose distribution in water differed from the calculated ones in tissue phantoms due to the densities and atomic composition for tissues that are not taken account by the TG-60 formalism.

J Contemp Brachytherapy 2019; 11, 1: 76-90
DOI: https://doi.org/10.5114/jcb.2019.83002

Key words: brachytherapy, AAPM TG-60, dosimetry, 32P, FLUKA.

Purpose

Brachytherapy is one type of internal radiation therapy used for cancer treatment, in which sealed radiation sources (e.g., needles, seeds, or capsules) are placed in short-distance from the target volume or directly into the area of the patient body that requires treatment [1,2]. Brachytherapy treatments can be classified according to different criteria including, implant methods, implant duration, loading systems, and radiation dose rate delivered by β and γ emission [3,4]. In comparison to the gamma emitter sources, β-emitters are proper candidates for some types of brachytherapy treatment (such as in intravascular coronary brachytherapy, treatment of metastatic uveal melanoma, and treatment of malignant hepatic lesions) due to the short range of electrons in tissue, resulting in a rapid decrease of deposited energy with a distance, with a sharp dose gradient [5,6]. 106Ru/106Rh, 90Sr/90Y, 90Y, and 32P are some common type of β-emitting radionuclides, which have good properties for the use in brachytherapy.

32P is a pure β emitter, with a 14.3-day half-life, maximum β energy of 1.71 MeV (average energy of 0.695 MeV), and with a maximum range of 76 mm in water/tissue [7]. It can be produced in a nuclear reactor by irradiation of sulfur-32, with moderately fast neutrons [8]. Recently, a new design of 32P brachytherapy source manufactured by the College of Chemistry of Sichuan University became available for the use in interstitial brachytherapy applications. Dosimetric characteristics of the source have been presented in a water phantom in detail by Junxiang *et al*. [9] by using the GEANT4 simulation code. According to the American Association of Physicists in Medicine (AAPM), theoretical and experimental determination of dosimetric characteristics of brachytherapy sources is essential for precise brachytherapy planning and dose distribution [10]. For β-emitting sources, AAPM TG-60/TG-149 report provides recommendations for dosimetry protocol within millimeter distances and review of intravascular brachytherapy physics. These dosimetric parameters include the reference absorbed

Address for correspondence: Payvand Taherparvar, Assist. Prof., Faculty of Science, Physics Department, University of Guilan, Namjoo Avenue, P.O. Box 41335-19141, 4193833697 Rasht, Guilan, Iran,
✉ e-mail: p.taherparvar@guilan.ac.ir, p.taherparvar@gmail.com

Received: 21.09.2018
Accepted: 03.02.2019
Published: 28.02.2019

dose, radial dose function, and anisotropy function [5,9]. Furthermore, the AAPM has recommended that the dosimetric parameters of brachytherapy sources should be obtained by two methods: simulation techniques and experimental measurements [11]. Because of the high gradient dose near the β-emitting brachytherapy sources and short range of the β particles, experimental determination of the dose deposition of these sources is very complicated. Then, it is desirable to use the Monte Carlo (MC) simulation methods to improve the accuracy of the dose calculation [2,12].

Monte Carlo methods are involved in many applications in nuclear medicine, such as nuclear medicine imaging (SPECT) [13] and radiation therapy (brachytherapy) [1,2,3,4,5]. The MC technique for brachytherapy applications is used as a tool for evaluation and validation of dose distribution in phantoms and patient anatomy as well as some useful dosimetric parameters such as dose distribution function, radial dose variation, and dose calculation at the reference point, according to the standard protocols by using random numbers [14]. Several different MC codes (MCNP, EGSnrc, GEANT4, FLUKA, PENELOPE, and GATE) have been utilized to evaluate dosimetric parameters of the most commonly used β-emitting sources in intravascular brachytherapy, which is described as follows.

Anjomrouz *et al*. [10] investigated the capability of the MC code FLUKA for the evaluation of the dosimetric parameters of 142Pr glass seed. Junxiang *et al*. [5] evaluated the dosimetric parameters of a new 90Y source in afterloading system by using the GEANT4 code. Kiavar and Sadeghi [15] calculated dose distribution in water for a pure β-emitting 32P intravascular brachytherapy (IVBT) stent by using the MCNP4C MC code and compared their simulation results with Carter *et al*. reported data [16]. Experimental measurements and simulation results of the radial dose function of 90Sr/90Y IVBT source were performed by Holmes *et al*. [17]. Dosimetry measurements for a 32P catheter-based vascular brachytherapy source wire using both radiochromic film and a plastic scintillator were performed by Mourtada *et al*. [18] and compared with MC calculations. Torres *et al*. [19] provided the complete dosimetric characteristics of a 32P IVBT source wires, with the PENELOPE and GEANT4 codes. MC calculation with the PENELOPE code was performed to obtain dosimetric parameters of a high-dose-rate 90Sr–90Y source by Asenjo *et al*. [20]. Wang *et al*. [21] employed EGS4 to derive the dosimetric parameters of 90Sr/90Y and 192Ir SS sources. Choi *et al*. [6] provided experimental simulation of the dosimetric characteristics of a new 32P ophthalmic applicator.

In the present study, we employed FLUKA MC code to derive accurate calculations of the dosimetric parameters of the new 32P source, following the formalism proposed by AAPM report TG-60, and an away-along table for the quality assurance (QA) purposes of the new 32P source. To ensure accuracy of calculations, our results were compared with the simulation results obtained by using the GEANT4 code, which were presented by Junxiang *et al*. [9]. The depth dose rate and radial dose function were also calculated for the sheathed 32P source.

Since the density, scattering coefficient, and absorption coefficient of the human body tissues are different from those of water, evaluation of the dosimetric parameters in the water phantom, which is considered in the TG-60 report, would be the cause of uncertainties in the dose calculations in the radiation therapy treatments. Because of the MC calculations of dose distribution for the new 32P in the body tissues are still unknown, we studied and compared the radial dose functions of the unsheathed and sheathed 32P sources, calculated for different media including liver, fat tissue, 9-component soft tissue, and 4-component soft tissue by means of the FLUKA MC code.

Material and methods

Monte Carlo simulation

In this study, the FLUKA code version 2011.2c-6 was utilized to evaluate the dose distributions around the new 32P source. FLUKA is a general-purpose MC particle transport code, which is based on the FORTRAN77 language, developed by a collaboration between INFN (Istituto Nazionale di Fisica Nucleare) and CERN (the European Council for Nuclear Research) [22]. The FLUKA MC code is a useful research tool for different areas of radiation therapy to simulate radiation transport in medium and through the human body for applications in radiation protection and dosimetry assessment [10,22,23,24,25]. Accurate geometry of the new 32P source was simulated by the FLUKA, which are shown schematically in Figure 1A and 1B for the sources unsheathed and sheathed by the catheter, respectively. The new 32P source has an active length of 0.47 cm, which is encapsulated inside a Teflon cylinder with a length of 0.42 cm, an internal and external diameter of 0.05 and 0.08 cm, respectively. It is welded by semi-spheres with the same diameters. The catheter is also made of Nylon-12. The space between the source and the catheter is filled with air [9].

The 32P β spectrum was defined according to ICRU Report No. 56, as illustrated in Figure 2 [26]. Then, the simulated sealed 32P brachytherapy source was located at the center of a spherical water phantom with a 30 cm radius to calculate dosimetric parameters according to AAPM report TG-60. In the simulation process, EM-CASCA option was chosen to consider electromagnetic cascades interactions. This option consists of "Landau-Pomeranchuk-Migdal effect and a special treatment of the tip of the bremsstrahlung spectrum" [22]. By use of the EM-CASCA option, Rayleigh scattering was also included in the simulation process. Furthermore, detailed transport of the electrons, positrons, and photons were considered with ElectroMagnetic FLUKA (EMF) card [27], without using any variance reduction techniques. The energy cut was set to 1ke, with EMFCUT card for electrons, positrons, and photons [27]. The uncertainties reported in our work were calculated from the statistical uncertainties from FLUKA output, and were computed according to the methods described by DeWerd *et al*. [28] for the dosimetric parameters.

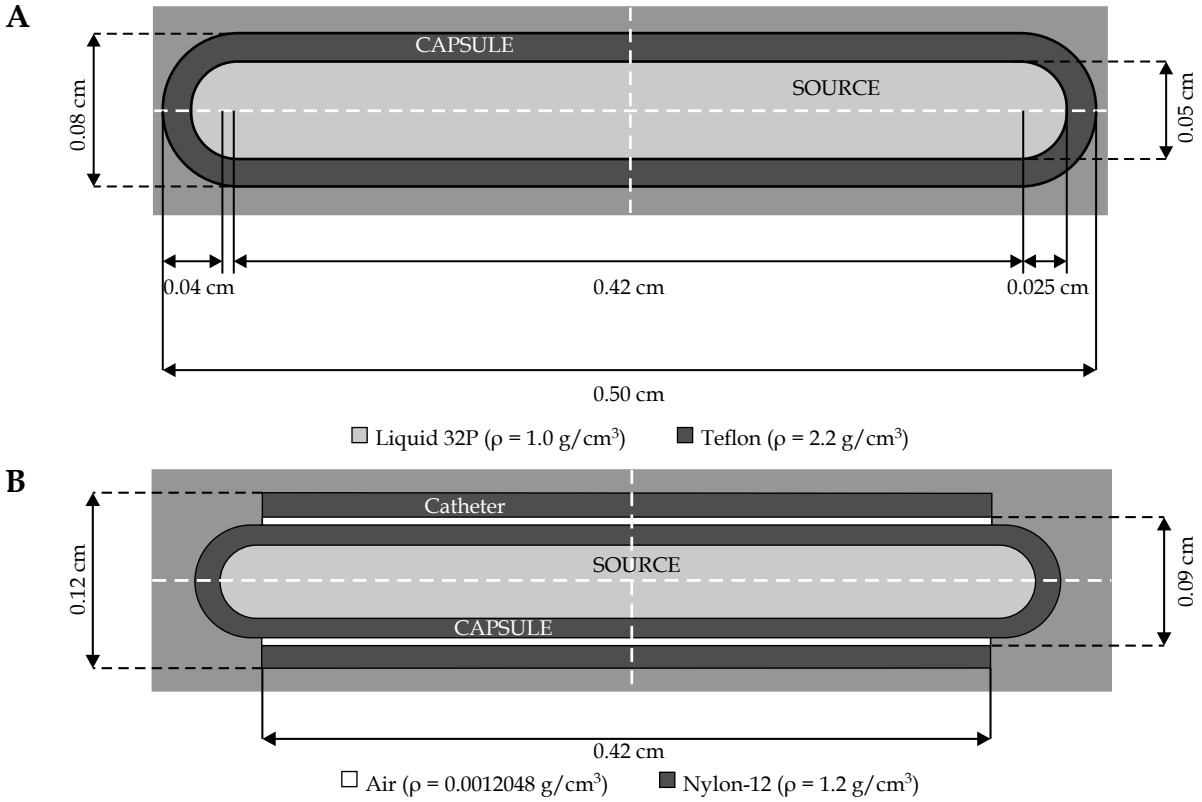

Fig. 1. Schematic design of the new 32P source: (**A**) unsheathed source and (**B**) sheathed source

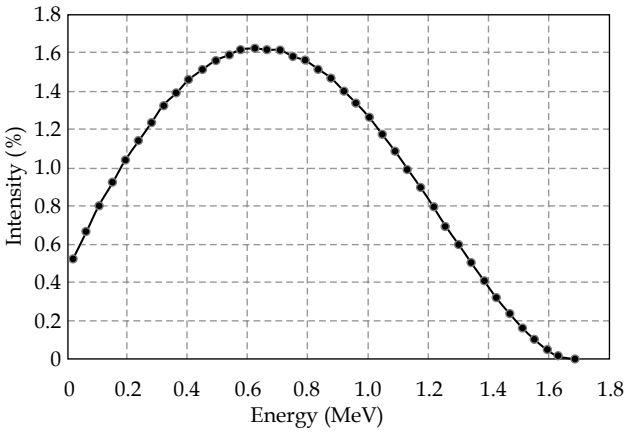

Fig. 2. Energy spectrum of the 32P source used in the FLUKA code

Dose calculation formalism

The reference dose rate ($\dot{D}(r_0,\theta_0)$), the radial dose function ($g_L(r)$), and the anisotropy function ($F(r,\theta)$) were calculated based on the AAPM report TG-60 recommendations for β-emitting brachytherapy sources. In this formalism, the absorbed dose rate in the water phantom is considered at the reference point, $\dot{D}(r_0,\theta_0)$, which is located at a radial distance of r_0 = 2 mm and a polar angle of $\theta_0 = \frac{\pi}{2}$ [5,29].

In our simulation, dose calculations were performed within voxels and were taken to be annular bins with radial thickness of 0.10 mm and height of 0.20 mm, according to the procedure described in Torres *et al*. [19] and Wang *et al*. [21]. The MC simulations were performed with 3 × 10^8 primary histories, and the maximum statistical uncertainty in our study for the dose calculation in water phantom was 0.35%. It should be noted that there are fairly large uncertainties in the dose measurements in experimental studies. In reference, Xu *et al*. [30] measured the dose distribution around a 3 mm long 32P source by using LiF thermoluminescent dosimeters and a scintillation detector. They point out that the uncertainties in the determination of the source activity, dose determination by the thermoluminescent dosimeters, and uncertainty in accounting for the detector geometry were about ±10%, ±5%, and ±5%, respectively. In addition, they mentioned that uncertainties in the detector position could yield a large uncertainty in the dose measurement (a shift of 0.10 mm changes the dose by 14% at a radial distance of 1.5 mm) due to the very steep dose gradient [29], while MC simulation does not include any of the mentioned experimental imperfections, which could improve the precision of the calculated values compared with the measured ones.

Results and discussion

Unsheathed source

Reference absorbed dose rate

The dose rate at the reference point was calculated for the new 32P source by using the FLUKA code, and it was determined to be about 1.3419 cGy $s^{-1}mCi^{-1}$ and 3.6266 × 10^{-10} in the terms of Gy/electron. The result is found to

Table 1. Comparison of the dose rate at the reference point from this work with calculated values of other study

	This work (FLUKA)	Junxiang *et al.* [9] (GEANT4)	Percentage difference
$\dot{D}(r_0,\theta_0)$(cGy s^{-1}mCi^{-1})	1.3419 ± 0.0006	1.2660 ± 0.0006	6.00%
$\dot{D}(r_0,\theta_0)$(Gy per electron)	3.6266×10^{-10}	3.4216×10^{-10}	6.00%

be in good agreement with the value calculated by Junxiang *et al.* [9], with a percentage difference of 6.00%. The results are presented in Table 1.

Radial dose function

Table 2 presents the results of the radial dose function for the simulated new 32P source at various radial distances from the source center. The percentage differences between the radial dose function calculated by the MC codes FLUKA and GEANT4 (Junxiang *et al.* [9]) were also listed in the last column in Table 2. As shown in this table, the obtained results are in excellent agreement with GEANT4 simulation at distances less than 3 cm from the source center. The differences between $g_L(r)$ results increase with increasing distance from the source center, with a maximum relative difference of 8.44% at r = 0.50 cm. In addition, a fifth-order polynomial equation, as expressed by Equation (1), is fit to the acquired values of $g_L(r)$ in the water phantom in the range of 0.10 to 0.50 cm.

Table 2. MC calculated radial dose function $g_L(r)$ of the new 32P source along with percentage differences between our study and Junxiang et al. [9] results

r (cm)	This work	Percentage difference
0.10	1.3884 ± 0.0009	0.97%
0.11	1.3558 ± 0.0009	–0.03%
0.12	1.3212 ± 0.0009	0.04%
0.13	1.2840 ± 0.0008	0.36%
0.14	1.2460 ± 0.0009	0.54%
0.15	1.2073 ± 0.0008	0.49%
0.16	1.1671 ± 0.0009	0.49%
0.17	1.1260 ± 0.0008	0.52%
0.18	1.0843 ± 0.0007	0.41%
0.19	1.0426 ± 0.0007	0.14%
0.20	1.0000 ± 0.0006	0.00%
0.21	0.9558 ± 0.0007	–0.06%
0.22	0.9136 ± 0.0007	–0.29%
0.23	0.8720 ± 0.0008	–0.73%
0.24	0.8298 ± 0.0008	–1.12%
0.25	0.7862 ± 0.0007	–1.22%
0.26	0.7458 ± 0.0006	–1.64%
0.27	0.7041 ± 0.0007	–1.68%
0.28	0.6629 ± 0.0005	–1.75%
0.29	0.6242 ± 0.0006	–1.96%
0.30	0.5857 ± 0.0005	–2.04%
0.35	0.4095 ± 0.0005	–1.53%
0.40	0.2666 ± 0.0004	–0.04%
0.45	0.1597 ± 0.0004	3.56%
0.50	0.0868 ± 0.0003	8.44%

$$g_L(r) = a_0 + a_1 r + a_2 r^2 + a_3 r^3 + a_4 r^4 + a_5 r^5 \quad (1),$$

where the coefficients of the radial dose function are determined as follows:

a_0 = 1.5753, a_1 = –0.1523 ($\frac{1}{\text{cm}}$), a_2 = –20.9231 ($\frac{1}{\text{cm}^2}$), a_3 = 38.9792 ($\frac{1}{\text{cm}^3}$), a_4 = –9.6679 ($\frac{1}{\text{cm}^4}$) and a_5 = –14.3910 ($\frac{1}{\text{cm}^5}$), and R^2 = 1.

Moreover, in our simulation, we used EMFFIX card, which is corresponding to the electron step sizes [27]. Differences in the running time between the simulations with and without the EMFFIX card is negligible. As shown in Figure 3, the values of the $g_L(r)$ along the radial axis with and without this card are similar, with a maximum difference of 0.49%.

Anisotropy function

The anisotropy function of the 32P brachytherapy source was calculated in the water phantom for the θ val-

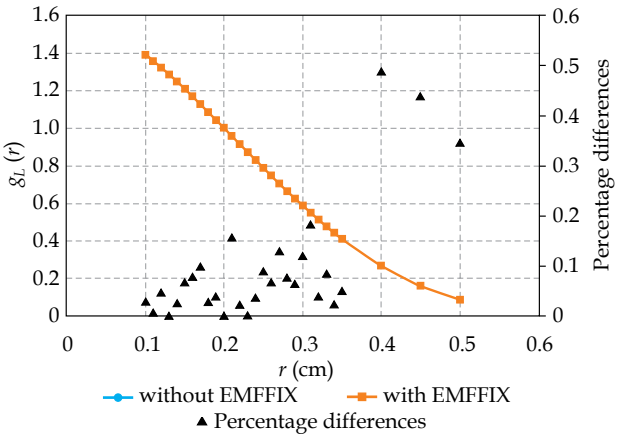

Fig. 3. Radial dose function of 32P source acquired with and without EMFFIX card along with their percentage differences

ues, ranging from 0° to 90° in 5-degree increments at 0.10-0.35 cm distances (in 0.01 cm increments) from the source center. The values of the simulated 2D anisotropy function of the new 32P source are shown in Table 3. The percentage differences between the values of the calculated anisotropy function in this study and the calculated ones with GEANT4 (Junxiang *et al*. [9]) were less than 6.0% at distances below 0.25 cm. The maximum percentage difference between FLUKA and GEANT4 results was about 14.0% for the distances ranging from 0.26 cm to 0.35 cm, at angles larger than 20°. In total, the two-dimensional anisotropy function is in good agreement with Junxiang *et al*. [9] simulation results.

Quality assurance

Implementing a QA program is an important step in brachytherapy plan to ensure accurate and reliable delivery of the prescribed dose to the target volume [31]. The QA program includes the quality control of the radiation sources and treatment planning calculation algorithms. The dosimetric characteristics of the brachytherapy sources, clinical dosimetry methods, and equipment to be applied have been well recommended by the AAPM Task Group 43 [32,33]. For treatment planning system (TPS) quality assurance purposes, the QA away-along data (gray per minute millicurie) of the new 32P source is presented in Table 4, for $0.00 \leq z \leq 0.40$ cm and $0.10 \leq y \leq 0.40$ cm, with increments of 0.20 cm. These results are used to calculate the dose rate distribution as a function of distance away from the source center in the Cartesian coordinate. A maximum relative difference of 11.9% ($z = 0.16$ cm, $y = 0.38$ cm) is observed, comparing to Junxiang *et al*. [9] results (with GEANT4). The statistical uncertainty was within 0.29%.

Dose profiles

Axial dose profiles, which is normalized to the reference point ($z = 0$, $y = 0.20$ cm), are shown in Figure 4A for the unsheathed 32P source at radial distances (y-distances) of 0.10, 0.15, 0.20, 0.25, 0.40, and 0.50 cm. Furthermore, Figure 4B shows normalized radial dose profiles of the 32P source at selected axial distances of 0, 0.10, 0.20, 0.25, 0.40, and 0.50 cm. Results show that the axial and radial dose profiles are relatively uniform; for $y \geq 0.20$ cm and $z > 0.25$ cm in the Figure 4A and 4B, respectively.

For small selected radial distances ($y < 0.40$), dose decreases rapidly as z-distance increases. As y-distance increases, the dose fall-off becomes shallower at the larger axial distances from the half-length of the source core. The radial dose profiles in Figure 4B shows that radial doses decline in an approximately exponential manner, as described by Junxiang *et al*. [9]. Radial doses, for small values of radial distances ($y < 0.25$ cm), drops off more sharply than for regions belong to $y > 0.25$ cm, especially at small axial distances.

Sheathed source

When a source is placed inside a catheter, the effects of the catheter material should be considered on the source strength and dose rate, due to the radiation absorption and scattering by the catheter. Therefore, we investigated the effect of the catheter on the dose rate distribution of the new 32P source. The results of the depth dose evaluation for the sheathed and unsheathed sources are presented in Table 5. Our results show that the depth dose results for the sheathed source are higher than the unsheathed source at all distances. Our simulation results and those provided by Junxiang *et al*. [9] simulation (by GEANT4) are presented in Figure 5 along with their percentage differences. Results demonstrate that the mean differences are about 5.05% and 5.67% for sheathed and unsheathed sources, respectively.

The effect of phantom material on the radial dose function

Unsheathed source

Since the attenuation coefficient of water is somewhat different from that of the human tissues, the water phantom for evaluation of dosimetric parameters may cause significant uncertainties in dose estimation around the brachytherapy sources in the TPS [34]. Since dose distribution for the new 32P in tissues is unknown, radial dose functions were calculated in four spherical phantoms consists of several types of human tissues: liver, fat tissue, 9-component soft tissue, and 4-component soft tissue. The tissue components were adopted from the report No. 44 of the International Commission on Radiation Units and Measurements (ICRU) [35].

Table 6 shows the dose rate values, in cGy s^{-1} mCi^{-1}, along the radial axis of the source for water and for several tissue phantoms. The maximum statistical uncertainties in dose calculations in the tissue phantoms were less than 0.51% for distances less than 0.3 cm and increased to 1.50% at larger distances.

Results show that the deposited dose decreases by increasing radial distance, as the energy of β particles are decreased, for all of the cases studied. Furthermore, the results of the radial dose function in liver, fat tissue, soft tissues, and water are shown in Figure 6. The simulation results indicate that the differences in the density and composition of the various tissues lead to changes in the deposited dose around a 32P source. Increasing differences between the radial dose functions calculated for different tissue phantoms, with increasing the distance from the source center, are notable. Figure 7 shows relative differences between the radial dose function of the 32P source obtained in the water phantom and that obtained for tissue phantom, which is calculated by Equation (2) for all tissues studied here.

$$[g_L(r)_{water} - g_L(r)_{tissue}]/g_L(r)_{water} \ \% \quad (2).$$

The maximum relative differences in various media were about 26.96%, 38.48%, 27.30%, 3.69% for liver, fat tissue, soft 9-component tissue, and soft 4-component tissue, respectively. Our results show that the differences between the results of $g_L(r)$ obtained in liver and 9-component soft tissue as well as 4-component soft tissue and

Table 3. Anisotropy function calculated for the new 32P source using the FLUKA code

θ (°)/r (cm)	0.10	0.11	0.12	0.13	0.14	0.15	0.16
0							
5							
10							
15							1.225
20			1.103	1.166	1.185	1.227	1.224
25	1.127	1.094	1.127	1.153	1.133	1.177	1.190
30	1.085	1.108	1.100	1.099	1.121	1.157	1.172
35	1.085	1.092	1.097	1.101	1.089	1.138	1.148
40	1.071	1.044	1.086	1.082	1.097	1.118	1.126
45	1.047	1.053	1.041	1.073	1.051	1.093	1.074
50	1.032	1.051	1.033	1.051	1.056	1.079	1.080
55	1.026	1.041	1.045	1.056	1.046	1.059	1.064
60	1.018	1.034	1.031	1.031	1.046	1.045	1.045
65	1.010	0.972	1.019	1.023	0.995	1.033	1.039
70	1.011	1.015	1.010	1.011	0.984	1.067	1.031
75	1.001	1.012	1.000	1.004	0.978	1.056	1.012
80	0.996	1.009	1.004	0.999	1.002	1.056	1.024
85	1.058	1.038	0.998	1.013	1.014	1.070	1.023
90	1.000	1.000	1.000	1.000	1.000	1.000	1.000
θ (°)/r (cm)	0.17	0.18	0.19	0.20	0.21	0.22	0.23
0							
5							
10							
15	1.359	1.257	1.277	1.418	1.248	1.206	1.183
20	1.245	1.255	1.253	1.278	1.255	1.255	1.249
25	1.215	1.248	1.277	1.323	1.249	1.337	1.297
30	1.194	1.224	1.217	1.225	1.234	1.336	1.261
35	1.158	1.182	1.223	1.195	1.205	1.238	1.241
40	1.138	1.146	1.162	1.224	1.186	1.203	1.213
45	1.113	1.133	1.143	1.159	1.170	1.175	1.171
50	1.087	1.096	1.104	1.120	1.130	1.150	1.149
55	1.056	1.096	1.094	1.101	1.103	1.112	1.139
60	1.128	1.060	1.073	1.114	1.077	1.076	1.095
65	1.042	1.052	1.050	1.071	1.078	1.067	1.089
70	1.024	1.032	1.024	1.033	1.044	1.034	1.040
75	1.018	1.014	1.016	1.023	1.022	1.032	1.039
80	1.020	1.021	1.008	1.009	1.033	1.006	1.004
85	1.008	1.030	1.013	1.014	1.008	1.009	1.010
90	1.000	1.000	1.000	1.000	1.000	1.000	1.000

Table 3. Cont.

θ (°)/r (cm)	0.24	0.25	0.26	0.27	0.28	0.29	0.30
0			0.866	1.031	1.145	1.244	1.406
5			1.080	1.115	1.178	1.269	1.462
10		1.321	1.225	1.171	1.225	1.302	1.612
15	1.614	1.460	1.367	1.367	1.299	1.706	1.629
20	1.254	1.484	1.568	1.318	1.453	1.374	1.646
25	1.293	1.490	1.442	1.449	1.361	1.376	1.663
30	1.448	1.346	1.447	1.325	1.375	1.455	1.620
35	1.245	1.281	1.318	1.327	1.398	1.340	1.588
40	1.296	1.316	1.336	1.356	1.378	1.308	1.418
45	1.183	1.240	1.214	1.225	1.239	1.277	1.272
50	1.155	1.188	1.180	1.212	1.201	1.250	1.270
55	1.175	1.172	1.142	1.149	1.167	1.252	1.218
60	1.116	1.163	1.114	1.111	1.125	1.256	1.269
65	1.070	1.100	1.079	1.074	1.081	1.150	1.187
70	1.037	1.078	1.056	1.064	1.094	1.051	1.166
75	1.035	1.055	1.056	1.027	1.078	1.034	1.111
80	1.014	1.047	1.014	1.011	1.026	1.030	1.072
85	1.003	1.038	1.096	1.003	1.036	1.041	1.063
90	1.000	1.000	1.000	1.000	1.000	1.000	1.000
θ (°)/r (cm)	0.31	0.32	0.33	0.34	0.35		
0	0.667	0.794	1.509	1.615	1.640		
5	1.384	1.009	1.748	1.627	1.637		
10	1.489	1.305	1.848	1.610	1.618		
15	1.581	1.900	1.518	1.619	1.656		
20	1.673	1.678	1.520	1.602	1.614		
25	1.717	1.668	1.518	1.582	1.592		
30	1.720	1.656	1.509	1.638	1.540		
35	1.334	1.665	1.479	1.580	1.485		
40	1.640	1.458	1.478	1.496	1.472		
45	1.282	1.466	1.343	1.390	1.376		
50	1.359	1.512	1.259	1.312	1.390		
55	1.184	1.430	1.298	1.305	1.238		
60	1.220	1.354	1.156	1.202	1.253		
65	1.213	1.171	1.187	1.165	1.142		
70	1.190	1.144	1.072	1.166	1.091		
75	1.135	1.103	1.043	1.078	1.084		
80	1.103	1.093	1.059	1.044	1.099		
85	1.069	1.071	1.067	1.028	1.108		
90	1.000	1.000	1.000	1.000	1.000		

Table 4. QA away-along data (Gy/(min mCi)) for the unsheathed 32P sources (*z* and *y* in cm)

y	*z* = 0.00	*z* = 0.10	*z* = 0.12	*z* = 0.14
0.10	2.845	2.774	2.666	2.490
0.12	2.134	2.056	1.956	1.839
0.14	1.707	1.551	1.423	1.387
0.16	1.316	1.194	1.135	1.066
0.18	1.070	0.925	0.881	0.818
0.20	0.805	0.711	0.676	0.640
0.22	0.633	0.569	0.533	0.498
0.24	0.498	0.447	0.426	0.391
0.26	0.356	0.352	0.320	0.316
0.28	0.308	0.277	0.249	0.249
0.30	0.241	0.213	0.206	0.178
0.32	0.178	0.170	0.162	0.142
0.34	0.142	0.132	0.124	0.107
0.36	0.107	0.102	0.096	0.092
0.38	0.087	0.071	0.071	0.071
0.40	0.066	0.059	0.057	0.053
y	*z* = 0.16	*z* = 0.18	*z* = 0.20	*z* = 0.22
0.10	2.302	2.063	1.778	1.475
0.12	1.692	1.529	1.331	1.138
0.14	1.279	1.156	1.067	0.889
0.16	0.985	0.889	0.796	0.697
0.18	0.765	0.697	0.626	0.553
0.20	0.601	0.533	0.496	0.427
0.22	0.462	0.427	0.391	0.352
0.24	0.373	0.344	0.313	0.281
0.26	0.285	0.272	0.249	0.213
0.28	0.231	0.213	0.196	0.177
0.30	0.178	0.169	0.142	0.140
0.32	0.142	0.132	0.121	0.107
0.34	0.107	0.103	0.095	0.085
0.36	0.071	0.071	0.074	0.066
0.38	0.066	0.060	0.057	0.050
0.40	0.050	0.046	0.043	0.036
y	*z* = 0.24	*z* = 0.26	*z* = 0.28	*z* = 0.30
0.10	1.209	0.960	0.747	0.711
0.12	0.941	0.782	0.619	0.498
0.14	0.749	0.640	0.513	0.427
0.16	0.605	0.509	0.427	0.356
0.18	0.481	0.427	0.356	0.292
0.20	0.386	0.334	0.285	0.242
0.22	0.309	0.271	0.233	0.198

Table 4. Cont.

y	*z* = 0.24	*z* = 0.26	*z* = 0.28	*z* = 0.30
0.24	0.249	0.219	0.188	0.162
0.26	0.199	0.176	0.153	0.132
0.28	0.159	0.140	0.121	0.106
0.30	0.124	0.112	0.098	0.085
0.32	0.099	0.088	0.078	0.068
0.34	0.071	0.069	0.060	0.053
0.36	0.060	0.054	0.046	0.042
0.38	0.046	0.042	0.036	0.032
0.40	0.035	0.032	0.028	0.025

y	*z* = 0.32	*z* = 0.34	*z* = 0.36	*z* = 0.38	*z* = 0.40
0.10	0.462	0.356	0.285	0.217	0.178
0.12	0.392	0.320	0.249	0.196	0.153
0.14	0.338	0.285	0.217	0.178	0.142
0.16	0.285	0.249	0.188	0.150	0.121
0.18	0.249	0.197	0.160	0.142	0.107
0.20	0.213	0.167	0.142	0.111	0.090
0.22	0.178	0.139	0.115	0.094	0.076
0.24	0.142	0.115	0.096	0.079	0.064
0.26	0.114	0.095	0.079	0.065	0.053
0.28	0.092	0.077	0.064	0.053	0.044
0.30	0.073	0.062	0.052	0.043	0.036
0.32	0.058	0.049	0.042	0.035	0.029
0.34	0.046	0.039	0.033	0.028	0.023
0.36	0.036	0.031	0.026	0.022	0.018
0.38	0.028	0.024	0.020	0.017	0.014
0.40	0.021	0.018	0.015	0.013	0.011

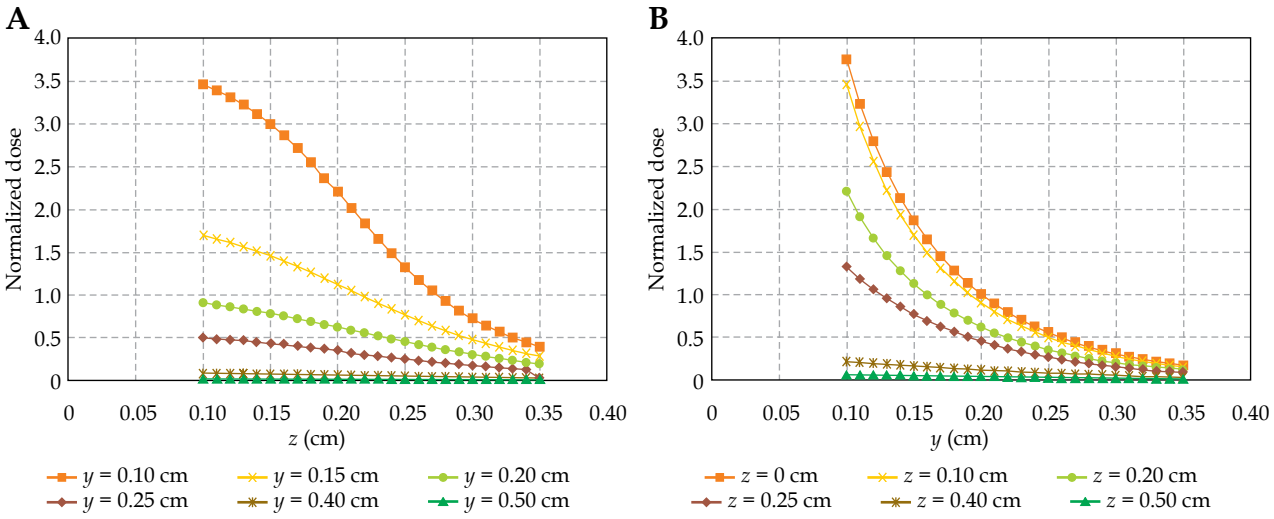

Fig. 4. **A**) Axial dose profiles with a different radial position, and (**B**) radial dose profiles with a different axial position, for the new 32P source in water

water are close to each other, which is due to having similar density and composition. Since the β particles emitted by 32P (with the average energy of 695 keV) have a maximum range of 0.76 cm in water, electrons with energies near the endpoint of the 32P β spectrum are responsible for differences between the radial dose functions in different media at large radial distances. In comparison with the gamma sources (such as 60Co [2]), differences between the radial dose functions calculated in the various tissue phantoms increased at small radial distances, which is due to short range of electrons than photons of the same energy.

Furthermore, we investigated dose rate × r^2 (cGy cm^2/s) parameter to eliminate the large variation at short distances caused by the inverse square law. The simulations were performed for the unsheathed source in the different tissue phantoms. As can be seen in Figure 8, the differences between the dose rate × r^2 results in water and in different media seems to increase at large radial distances from the center of the source, which also depend on the tissue type. A maximum difference of 44.49% was obtained at depth of 0.50 cm for fat tissue relative to the water.

Sheathed source

The calculation results of dose rate distributions for the sheathed source in different media are presented in Table 7. According to the results, it is evident that the dose rate distributions increased relatively to the unsheathed source in all cases.

The simulated radial dose functions of the sheathed source in different tissue phantoms are presented in Figure 9. As the depth increased, the radial dose function in different media decreased; for the fat tissue, $g_L(r)$ decreased at a slower rate than for water, whereas the function for liver and 9-component soft tissue decreased faster than for water.

The relative differences between the radial dose function of the sheathed source obtained in water phantom and that obtained for a tissue phantom (Equation 2) for all tissues studied here, as illustrated in Figure 10, show that the maximum relative differences occurred at the greatest radial distance from the source. The maximum relative differences were 26.20%, 37.76%, 25.63%, and 4.58% for liver, fat tissue, soft 9-component tissue, and soft 4-component tissue, respectively, which are less than calculated ones for the unsheathed source, with the exception of the soft 4-component tissue.

The result of dose rate × r^2 for the sheathed source in different media, as shown in Figure 11, is similar to that for the unsheathed source. The difference between $(\text{dose rate} \times r^2)_{\text{tissue}}$ and $(\text{dose rate} \times r^2)_{\text{water}}$ increased with increasing the radial distance; a maximum difference of 42.92% was showed at depth of 0.50 cm for fat tissue. The maximum differences between $(\text{dose rate} \times r^2)_{\text{tissue}}$ of the sheathed source and unsheathed source were about 2.96%, 0.88%, 1.67%, 4.68%, and 2.00% for liver, fat tissue, water, soft 9-component tissue, and soft 4-component tissue, respectively.

Since overall uncertainty of the delivered doses to the target volume should be less than ± 5% [31], the tissue effects on the radial dose function, as seen in Figure 10,

Table 5. Depth dose rate distributions (cGy/(s mCi)) calculated for the sheathed and unsheathed 32P sources

r (cm)	$\dot{D}(r,z_0)$	$\dot{D}_{\text{cath}}(r,z_0)$
0.10	5.0297	5.1089
0.11	4.3295	4.3897
0.12	3.7499	3.8001
0.13	3.2627	3.3055
0.14	2.8517	2.8872
0.15	2.5019	2.5297
0.16	2.2005	2.2269
0.17	1.9396	1.9625
0.18	1.7128	1.7312
0.19	1.5156	1.5298
0.20	1.3419	1.3547
0.21	1.1874	1.1997
0.22	1.0536	1.0636
0.23	0.9357	0.9433
0.24	0.8306	0.8367
0.25	0.7356	0.7418
0.26	0.6535	0.6577
0.27	0.5790	0.5837
0.28	0.5133	0.5180
0.29	0.4544	0.4583
0.30	0.4022	0.4062
0.31	0.3556	0.3590
0.32	0.3142	0.3174
0.33	0.2769	0.2801
0.34	0.2440	0.2461
0.35	0.2145	0.2165
0.36	0.1884	0.1906
0.37	0.1651	0.1676
0.38	0.1443	0.1460
0.39	0.1259	0.1279
0.40	0.1098	0.1115
0.41	0.0953	0.0968
0.42	0.0826	0.0840
0.43	0.0714	0.0726
0.44	0.0614	0.0625
0.45	0.0529	0.0538
0.46	0.0454	0.0462
0.47	0.0387	0.0394
0.48	0.0329	0.0335
0.49	0.0279	0.0285
0.50	0.0236	0.0240

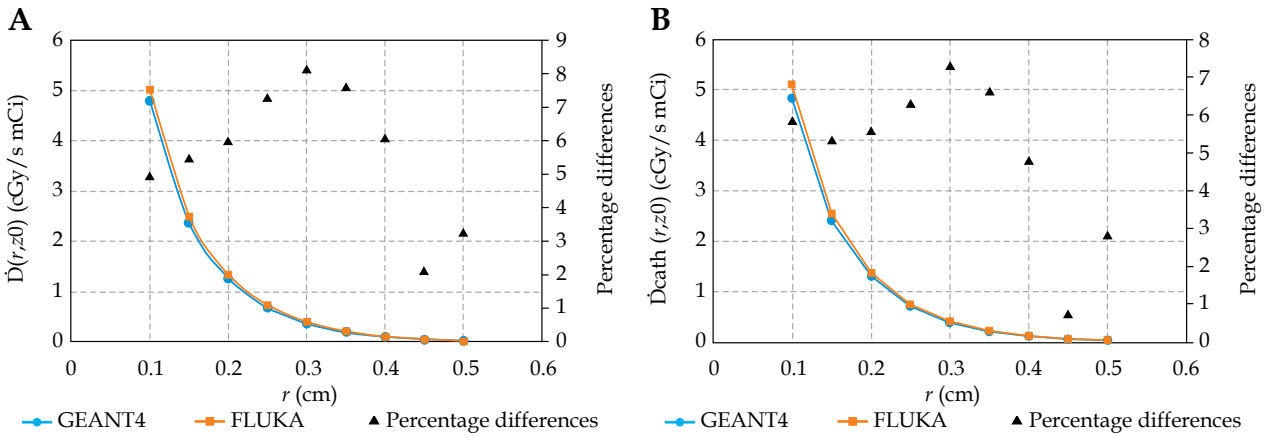

Fig. 5. Depth dose rate (cGy s^{-1} mCi^{-1}) obtained in water for (**A**) the unsheathed source and (**B**) the sheathed source calculated by FLUKA code, along with their percentage differences from the GEANT4 simulation results [9]

Table 6. Dose rate distributions (in cGy $s^{-1}mCi^{-1}$) for the unsheathed new 32P source calculated in different tissue phantoms

r (cm)	Liver	Fat	Soft tissue (9-component)	Soft tissue (4-component)
Density (g/cm^3)	1.06	0.95	1.06	1.00
0.10	4.9417	5.0312	4.9427	4.9946
0.11	4.2447	4.3420	4.2428	4.2993
0.12	3.6627	3.7746	3.6643	3.7250
0.13	3.1802	3.2963	3.1796	3.2444
0.14	2.7711	2.8929	2.7722	2.8404
0.15	2.4226	2.5478	2.4225	2.4913
0.16	2.1244	2.2499	2.1241	2.1924
0.17	1.8679	1.9942	1.8673	1.9359
0.18	1.6425	1.7688	1.6419	1.7103
0.19	1.4449	1.5728	1.4457	1.5121
0.20	1.2740	1.3994	1.2749	1.3407
0.21	1.1258	1.2464	1.1245	1.1906
0.22	0.9933	1.1122	0.9930	1.0560
0.23	0.8766	0.9914	0.8761	0.9371
0.24	0.7735	0.8853	0.7733	0.8325
0.25	0.6819	0.7910	0.6823	0.7394
0.26	0.6025	0.7058	0.6026	0.6564
0.27	0.5305	0.6310	0.5312	0.5829
0.28	0.4673	0.5633	0.4674	0.5167
0.29	0.4114	0.5030	0.4112	0.4584
0.30	0.3615	0.4480	0.3613	0.4061
0.35	0.1851	0.2507	0.1853	0.2182
0.40	0.0898	0.1356	0.0899	0.1129
0.45	0.0404	0.0703	0.0405	0.0548
0.50	0.0164	0.0341	0.0163	0.0245

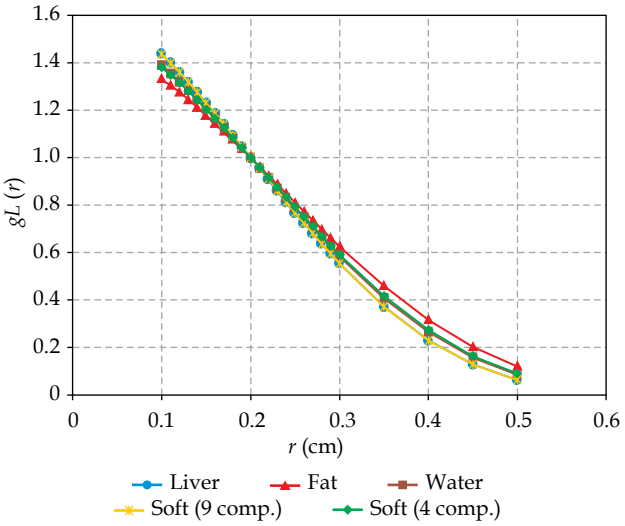

Fig. 6. Radial dose function obtained in different media for the new 32P unsheathed source

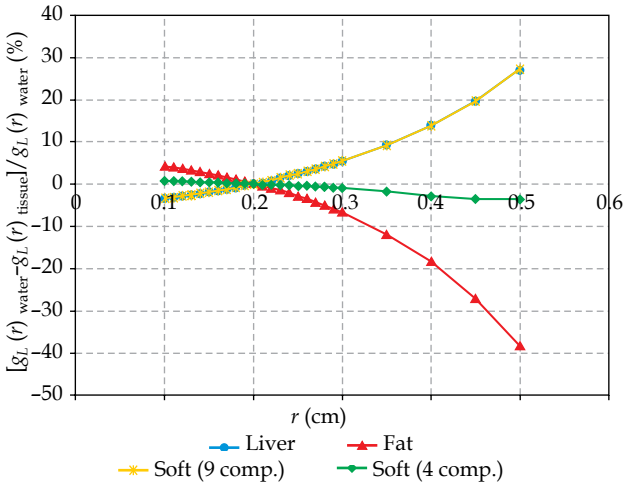

Fig. 7. Relative differences between the radial dose function of the unsheathed source obtained in the water phantom and that obtained for a tissue phantom, for liver, fat tissue, 9-component soft tissue, and 4-component soft tissue

are considerable at radial distances far from the source center (r > 0.20 cm) in the liver, fat tissue, and soft 9-component tissue. On the other hand, percentage differences between radial dose function in water and in soft 4-component tissue change up to 3.81% relative to water at all radial distances from the source center, which is within the recommended range.

Conclusions

In this study, we have presented the reference absorbed dose rate, the radial dose function, the two-dimensional anisotropy function, the normalized dose profiles, and the QA away-along look-up table calculation in tabulated and graphical format, by using the FLUKA code for the new 32P brachytherapy source according to TG-60 formalism. Our results have been compared to the values quoted in the published data using the GEANT4 simulation by Junxiang *et al.* [9]. Our results agreed quite well with GEANT4, which show the capability of FLUKA MC code in an accurate simulation of the new 32P brachytherapy source. We also studied the effect of the catheter on the dose distribution data in the water phantom, which showed an increase in the dose rate distributions on the central axis of the sheathed source.

Since dosimetric parameters of the brachytherapy sources according to the AAPM TG-60 formalism should be performed in a homogeneous water phantom, differences in density and atomic composition of the various tissues contained in the human body were not considered in this formalism. Then, we evaluated dose distribution of the sheathed and unsheathed 32P sources in different tissue phantoms including liver, fat tissue, and soft (9-component and 4-component) tissue by using FLUKA code, which has not been studied before.

Our results show that the absorbed dose rate in the various tissues decreased as radial distance increased in an approximately exponential way. Furthermore, the dose distribution produced by the 32P source in the various tissues will not be the same as water, so it could not correctly estimate the amount of radiation dose received by patients in clinical practice. The difference of absorbed doses calculated to the various tissues and to water, which is depending on the composition of the tissues, increases with increasing radial distance from the source. The maximum percentage difference between the radial dose function in different media is equal to 38.48%, which is related to the radial dose function calculated in fat tissue. Therefore, it is necessary to use the correction factors, which depend on the tissue type and compositions, in dosimetry protocols and TPS of new brachytherapy source. The differences between radial dose functions (and dose rate × r^2) in water and in different media were also observed for the sheathed and unsheathed sources. Results of dosimetric parameters for the sheathed and unsheathed sources indicate that

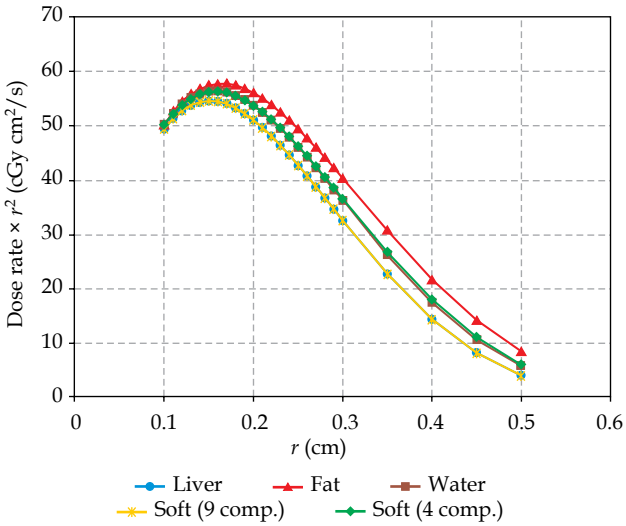

Fig. 8. Dose rate × r^2 along the radial axis obtained in different media for the unsheathed source calculated by FLUKA

Table 7. Dose rate distributions (in cGy $s^{-1}mCi^{-1}$) for the sheathed 32P source calculated in different tissue phantoms

r (cm)	Liver	Fat	Soft tissue (9-component)	Soft tissue (4-component)
Density (g/cm^3)	1.06	0.95	1.06	1.00
0.10	5.0379	5.0758	5.0417	5.0585
0.11	4.3224	4.3803	4.3198	4.3552
0.12	3.7313	3.8044	3.7285	3.7708
0.13	3.2351	3.3221	3.2331	3.2809
0.14	2.8151	2.9101	2.8162	2.8684
0.15	2.4614	2.5622	2.4625	2.5163
0.16	2.1579	2.2610	2.1564	2.2130
0.17	1.8929	2.0007	1.8923	1.9522
0.18	1.6655	1.7742	1.6655	1.7244
0.19	1.4669	1.5774	1.4667	1.5261
0.20	1.2930	1.4017	1.2930	1.3501
0.21	1.1413	1.2485	1.1412	1.1981
0.22	1.0081	1.1131	1.0077	1.0641
0.23	0.8895	0.9941	0.8896	0.9437
0.24	0.7851	0.8871	0.7859	0.8381
0.25	0.6934	0.7917	0.6937	0.7443
0.26	0.6112	0.7069	0.6115	0.6604
0.27	0.5392	0.6313	0.5394	0.5867
0.28	0.4753	0.5633	0.4754	0.5206
0.29	0.4183	0.5034	0.4189	0.4615
0.30	0.3677	0.4489	0.3680	0.4093
0.35	0.1889	0.2509	0.1887	0.2205
0.40	0.0921	0.1363	0.0920	0.1114
0.45	0.0416	0.0706	0.0420	0.0559
0.50	0.0169	0.0343	0.0171	0.0250

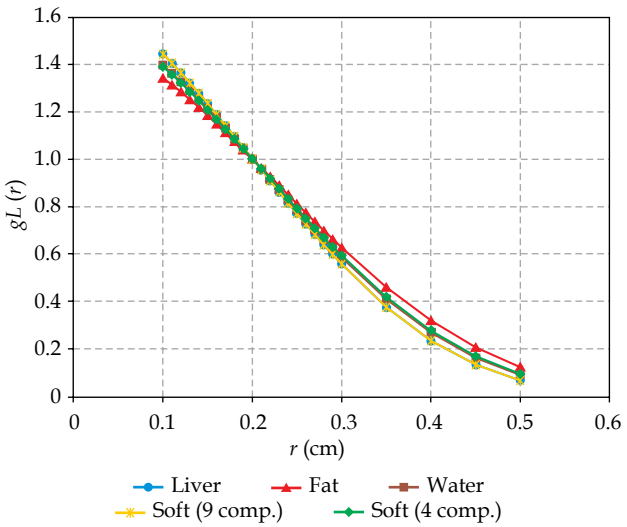

Fig. 9. Radial dose function calculated in different media for the new 32P sheathed source

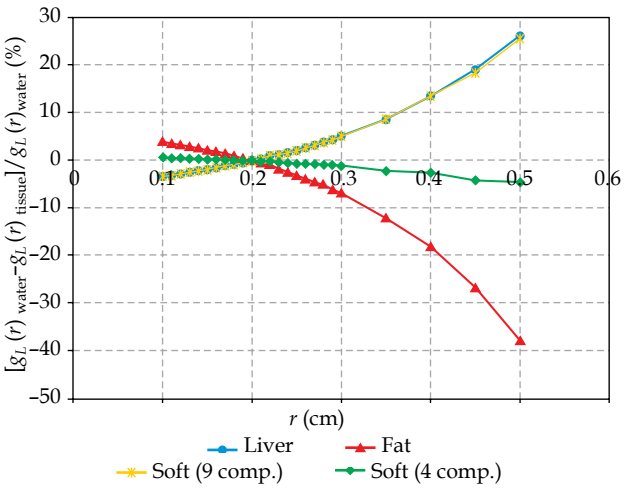

Fig. 10. Relative differences between the radial dose function of the sheathed source obtained in the water phantom and that obtained for a tissue phantom, for liver, fat tissue, 9-component soft tissue, and 4-component soft tissue

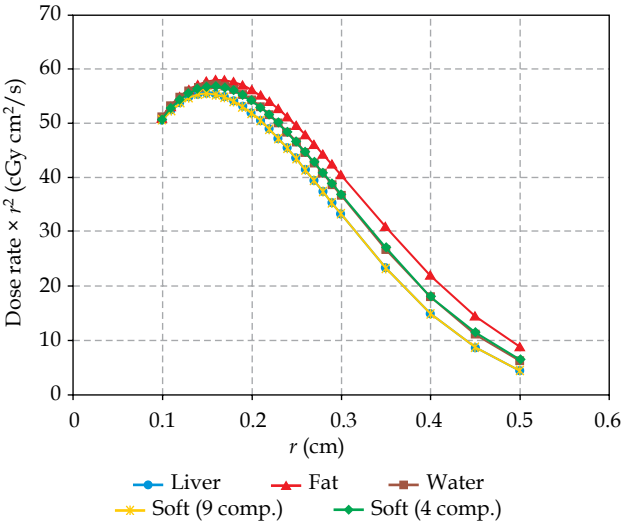

Fig. 11. Dose rate × r^2 along the radial axis obtained in different media for the sheathed source calculated by FLUKA code

tissue effects are considerable at large radial distances from the source center.

The results show that in the clinical brachytherapy of liver metastases by using the 32P sealed radioactive source placed within the liver, the dose rate distributions at short distances from the source is well-estimated by calculated ones according to the AAPM TG-60 formalism, which is performed in a water phantom. On the other hand, the calculation of dose rate of the 32P source in the water phantom may lead to inaccurate dose estimation in the long-distances from the source as well as in the adjacent organs. Acquired dosimetric characteristics of the new 32P source can be used as input data to verify the calculations of TPS for exact dose delivery to the patient in brachytherapy.

Disclosure

Authors report no conflict of interest.

References

1. Schaart DR. Sealed catheter-based beta sources for intravascular brachytherapy: novel designs and dosimetric characterization. Delft University Press 2002; 1-11.
2. Badry H, Oufni L, Ouabi H et al. A Monte Carlo investigation of the dose distribution for 60Co High Dose Rate brachytherapy source in water and in different media. *Appl Radiat Isot* 2018; 136: 104-110.
3. Pawlicki T, Scanderbeg DJ, Starkschall G. Hendee's radiation therapy physics. Wiley-Blackwell 2016; 215-230.
4. Thomadsen B, Rivard M, Butler W. Brachytherapy physics. *Med Phys* 2005: 1-5.
5. Junxiang W, Shihu Y, Jing H et al. Monte Carlo dosimetry of a new 90Y brachytherapy source. *J Contemp Brachytherapy* 2015; 7: 397-406.
6. Choi CH, Han HS, Son KJ et al. Dosimetry of a new P-32 ophthalmic applicator. *Med Phys* 2011; 38: 6143-6151.
7. Sun L, Zhu X, Xu L et al. Antitumor effects of 32P-chromic-poly (L-lactide) brachytherapy in nude mice with human prostate cancer. *Oncol Lett* 2013; 6: 687-692.
8. Lyra ME, Andreou M, Georgantzoglou A et al. Radionuclides used in nuclear medicine therapy – from production to dosimetry. *Curr Med Imaging Rev* 2013; 9: 51-75.
9. Junxiang W, Jing H, Fengxiang L et al. Monte Carlo dosimetric parameter study of a new 32P brachytherapy source. *Br J Radiol* 2016; 89: 1-9.
10. Anjomrouz M, Bakht MK, Sadeghi M. Feasibility study of FLUKA Monte Carlo simulation for a beta emitting brachytherapy source: dosimetric parameters of 142Pr glass seed. *J Radioanal Nucl Chem* 2016; 3: 947-953.
11. Sadeghi M, Taghdiri F, Saidi P. Dosimetric characteristics of the 192Ir high-dose-rate afterloading brachytherapy source. *Japan J Radiol* 2011; 29: 324-329.
12. Paiva E. Numerical calculation of relative dose rates from cylindrical 32P and 90Y beta sources used in intravascular brachytherapy. *Scientia Plena* 2014; 9: 1-12.
13. Taherparvar P, Sadremomtaz A. Development of GATE Monte Carlo simulation for a CsI pixelated gamma camera dedicated to high resolution animal SPECT. *Australas Phys Eng Sci Med* 2018; 41: 31-39.
14. Almansa López JF, Torres Donaire J, Guerrero Alcalde R. Monte Carlo dosimetry of the most commonly used 192Ir high dose rate brachytherapy sources. *Rev Fis Med* 2011; 12: 159-168.
15. Kiavar O, Sadeghi M. Modeling and dose calculations of a pure beta emitting 32P coated stent for intracoronary brachytherapy by Monte Carlo code. *Iran J Radiat Res* 2012; 9: 257-263.
16. Carter AJ, Laird JR. Experimental results with endovascular irradiation via a radioactive stent. *Int J Radiat Oncol Biol Phys* 1996; 36: 797-803.
17. Holmes SM, DeWerd LA, Micka JA. Experimental determination of the radial dose function of 90Sr/90Y IVBT sources. *Med Phys* 2006; 33: 3225-3233.
18. Mourtada FA, Soares CG, Seltzer SM et al. Dosimetry characterization of 32P catheter-based vascular brachytherapy source wire. *Med Phys* 2000; 27: 1770-1776.
19. Torres J, Buades MJ, Almansa JF et al. Dosimetry characterization of 32P intravascular brachytherapy source wires using Monte Carlo codes PENELOPE and GEANT4. *Med Phys* 2004; 31: 296-304.
20. Asenjo J, Fernández-Varea JM, Sánchez-Reyes A. Characterization of a high-dose-rate 90Sr–90Y source for intravascular brachytherapy by using the Monte Carlo code PENELOPE. *Phys Med Biol* 2002; 47: 697-711.
21. Wang R, Li XA. A Monte Carlo calculation of dosimetric parameters of 90Sr / 90Y and 192 Ir SS sources for intravascular brachytherapy. *Med Phys* 2000; 27: 2528-2535.
22. Cerutti F, Engel R, Fedynitch A et al. New developments in FLUKA. *NEA/NSC/R* 2015; 3: 220-230.
23. Cao Z, Ruan XC, Meng BD et al. Determination of dosimetric characteristics for 125I seed source with FLUKA code. *Nucl Sci Tech* 2014; 25: 1-3.
24. Demir N, Tarim UA, Popovici MA et al. Investigation of mass attenuation coefficients of water, concrete and bakelite at different energies using the FLUKA Monte Carlo code. *J Radioanal Nucl Chem* 2013; 2: 1303-1307.
25. Andersen V, Ballarini F, Battistoni G et al. The application of FLUKA to dosimetry and radiation therapy. *Radiat Prot Dosimetry* 2005; 116: 113-117.
26. ICRU Report No. 56. Dosimetry of external beta rays for radiation protection, International Commission on Radiation Units and Measurements, Bethesda, MD, 1997.
27. Ferrari A, Sala PR, Fasso A et al. Fluka: a multi-particle transport code. CERN 2005.
28. DeWerd LA, Ibbott GS, Meigooni AS et al. A dosimetric uncertainty analysis for photon-emitting brachytherapy sourc-

es: Report of AAPM Task Group No. 138 and GEC-ESTRO. *Med Phys* 2011; 38: 782- 801.
29. Chiu-Tsao ST, Schaart DR, Soares CG et al. Dose calculation formalisms and consensus dosimetry parameters for intravascular brachytherapy dosimetry: Recommendations of the AAPM Therapy Physics Committee Task Group No. 149. *Med Phys* 2007; 34: 4126-4157.
30. Xu Z, Almond PR, Deasy JO. The dose distribution produced by a 32P source for endovascular irradiation. *Int J Radiat Oncol Biol Phys* 1996; 36: 933-939.
31. Jursinic PA. Quality assurance measurements for high-dose-rate brachytherapy without film. *J Appl Clin Med Phys* 2014; 15: 246-261.
32. Aalbers AHL, De Brabandere M, Koedooder C et al. Dosimetry and quality control of brachytherapy with low-energy photon sources (125I). The Netherlands Commission on Radiation Dosimetry Subcommittee 2012.
33. Nath R, Amols H, Coffey C et al. Intravascular brachytherapy physics: Report of the AAPM Radiation Therapy Committee Task Group No. 60. *Med Phys* 1999; 26: 119-152.
34. Ghorbani M, Salahshour F, Haghparast A et al. Effect of tissue composition on dose distribution in brachytherapy with various photon emitting sources. *J Contemp Brachytherapy* 2014; 6: 54-67.
35. ICRU. ICRU Report No. 44, Tissue substitutes in radiation dosimetry and measurement. ICRU, Bethesda 1989.